MATHEMATICAL MODELLING
МАТЕМАТИЧЕСКОЕ МОДЕЛИРОВАНИЕ

UDC 519.6

Original Empirical Research

https://doi.org/10.23947/2587-8999-2025-9-3-44-55

Adaptive Grid Techniques for the Efficient Simulation of Shallow Coastal Systems

Alexander I. Sukhinov[1], Sofia V. Protsenko[2] ✉, Elena A. Protsenko[2]

[1] Don State Technical University, Rostov-on-Don, Russian Federation

[2] Taganrog Institute named after A.P. Chekhov (branch) of RSUE, Taganrog, Russian Federation

✉ rab55555@rambler.ru

Abstract

Introduction. Shallow coastal systems are highly dynamic and require accurate numerical models for predicting tides, storm surges, and coastal hazards. Traditional uniform-grid approaches often incur high computational costs, limiting their applicability for operational forecasting. Adaptive grid techniques provide a promising alternative by concentrating resolution in dynamically important regions while reducing the total computational burden.

Materials and Methods. We developed an adaptive-grid framework based on the depth-averaged shallow-water equations. The model employs a second-order finite-volume scheme with TVD limiting on a quadtree mesh. Mesh adaptation is driven by gradient indicators of free-surface elevation and velocity, ensuring high resolution in areas with steep gradients, tidal fronts, and complex bathymetry. Three numerical experiments were performed: a harmonic tide, a wind-driven storm surge, and combined tidal-wind forcing.

Results. The proposed method demonstrated robust wetting-drying capabilities, a mass conservation error below 0.06%, and skill metrics of RMSE ≤ 0.07 m and NSE ≥ 0.90. Compared to a uniform grid of the same finest resolution, Adaptive Mesh Refinement (AMR) reduced the mean cell count by ~32% and wall time by ~1.5×, with less than 3.5% change in the L_2 error norm.

Results. Numerical experiments have shown stable operation of the drainage and flooding algorithms, the mass conservation error did not exceed 0.06%. The qualitative characteristics of the model are confirmed by the values of the RMSE < 0.07 m and NSE > 0.90 metrics. A comparison with calculations on a uniform grid with a similar minimum step showed that the use of adaptive refinement (AMR) reduces the average number of calculation cells by about 32% and reduces machine time by 1.5 times with an increase in the error rate L_2 by less than 3.5%.

Discussion. The results confirm that adaptive meshing preserves physical accuracy while substantially reducing computational cost. This makes the method a suitable tool for high-resolution coastal hazard assessment and operational forecasting.

Conclusion. Further work will focus on extending the approach to three-dimensional flows and incorporating data assimilation for real-time applications.

Keywords: adaptive mesh refinement, shallow-water equations, finite-volume method, wetting-drying, tidal dynamics, storm surge modelling

Funding. The study was supported by the Russian Science Foundation grant No. 25–21–00021, https://rscf.ru/en/project/ 25-21-00021/

For Citation. Sukhinov A.I., Protsenko S.V., Protsenko E.A. Adaptive Grid Techniques for the Efficient Simulation of Shallow Coastal Systems. *Computational Mathematics and Information Technologies*. 2025;9(3):44–55. https://doi.org/10.23947/2587-8999-2025-9-3-44-55

Оригинальное эмпирическое исследование

Адаптивные сеточные методы для эффективного моделирования динамики мелководных прибрежных систем

А.И. Сухинов[1], **С.В. Проценко**[2] ✉, **Е.А. Проценко**[2]
[1] Донской государственный технический университет, г. Ростов-на-Дону, Российская Федерация
[2] Таганрогский институт имени А.П. Чехова (филиал) РГЭУ (РИНХ), г. Таганрог, Российская Федерация
✉ rab55555@rambler.ru

Аннотация

Введение. Мелководные прибрежные зоны представляют собой высокодинамичные природные системы, в которых протекают сложные гидродинамические процессы, обусловленные взаимодействием приливных явлений, ветрового воздействия и особенностей рельефа дна. Для их надежного прогнозирования и оценки связанных с ними экологических и техногенных рисков необходимы численные модели повышенной точности. Однако традиционные методы, основанные на использовании равномерных расчетных сеток, характеризуются чрезмерными вычислительными затратами, что существенно ограничивает их применение в задачах оперативного прогнозирования. В этой связи перспективным направлением является использование адаптивных сеточных методов, позволяющих сосредотачивать расчетное разрешение в динамически значимых областях и одновременно снижать общую вычислительную нагрузку.

Материалы и методы. Разработана численная модель, основанная на двумерных уравнениях мелкой воды в постановке с усреднением по глубине. В качестве расчетного алгоритма применена конечно-объемная схема второго порядка точности с TBD-лимитированием, реализованная на динамически адаптируемой сетке типа квадродерева. Критерием для локального уточнения сетки служат градиенты уровня свободной поверхности и скорости течений, что обеспечивает детальную аппроксимацию в зонах интенсивной динамики, включая приливные фронты и области со сложной батиметрией. Для оценки эффективности метода проведены три численных эксперимента: моделирование гармонического прилива, ветрового штормового нагона и их комбинированного воздействия.

Результаты исследования. Численные эксперименты показали устойчивую работу алгоритмов осушения и затопления, погрешность сохранения массы не превышала 0,06 %. Качественные характеристики модели подтверждаются значениями метрик RMSE ≤ 0,07 м и NSE ≥ 0,90. Сравнение с расчетами на равномерной сетке аналогичного минимального шага показало, что применение адаптивного уточнения (AMR) позволяет сократить среднее число расчетных ячеек примерно на 32 % и уменьшить машинное время в 1,5 раза при увеличении нормы погрешности L_2 менее чем на 3,5 %.

Обсуждение. Полученные результаты свидетельствуют о том, что использование адаптивных сеточных методов обеспечивает сохранение физической достоверности при значительном снижении вычислительных затрат. Это делает предложенный подход эффективным инструментом для высокоточного моделирования и прогноза гидродинамических процессов в прибрежных зонах, в том числе для оценки и предотвращения последствий опасных гидрометеорологических явлений.

Заключение. В дальнейшем предполагается развитие модели в направлении трехмерных расчетов и интеграции с методами ассимиляции данных, что позволит использовать ее для оперативных прогнозов в реальном времени.

Ключевые слова: адаптивное уточнение сетки, уравнения мелкой воды, конечно-объемный метод, осушение и затопление, приливная динамика, моделирование штормовых нагонов

Финансирование. Исследование выполнено за счет гранта Российского научного фонда № 25–21–00021, https://rscf.ru/en/project/ 25-21-00021/

Для цитирования. Сухинов А.И., Проценко С.В., Проценко Е.А. Адаптивные сеточные методы для эффективного моделирования динамики мелководных прибрежных систем. *Computational Mathematics and Information Technologies*. 2025;9(3):44–55. https://doi.org/10.23947/2587-8999-2025-9-3-44-55

Introduction. Shallow water environments such as coastal lagoons, estuaries, and shelf seas play a critical role in global biogeochemical cycles, marine ecosystems, and human activities. Accurate numerical simulation of these regions is essential for predicting storm surges, seiche waves, sediment transport, and pollutant dispersion, particularly under increasing anthropogenic and climatic pressures. However, the inherent complexity of shallow water domains — including variable bathymetry, rapidly changing flow regimes, and strong nonlinear interactions — poses significant challenges for traditional numerical models based on static mesh structures.

Recent advances in computational fluid dynamics (CFD) and environmental modelling have demonstrated the advantages of adaptive grid techniques for resolving multiscale flow structures with increased accuracy and efficiency. Adaptive grids enable localized mesh refinement in dynamically evolving regions of interest, thereby reducing computational cost without sacrificing solution fidelity. These techniques are particularly valuable in shallow water applications, where fine resolution is often required near coastlines, river mouths, and topographic gradients.

A variety of adaptive strategies have been proposed and implemented in both structured and unstructured frameworks. Structured block-based methods with static or dynamic refinement (e. g., nested grids or quadtree/octree hierarchies) are employed in models such as Delft3D Flexible Mesh and ADCIRC [3]. Unstructured adaptive meshes using Delaunay triangulation or Voronoi tessellation have gained traction in systems like TELEMAC, SLIM, and OpenFOAM [2]. Moreover, dynamic mesh adaptation guided by error estimators or flow gradients (e. g., vorticity, free surface slope) has been successfully applied to simulate storm surges and flooding scenarios with high spatial fidelity [1].

In addition to deterministic refinement criteria, recent developments incorporate machine learning to predict optimal refinement zones, as shown by Guo et al. (2023) in their hybrid neural network — CFD coupling for coastal flood prediction. Such approaches point to a future of intelligent, data-informed adaptive modelling systems [5].

Despite these advancements, a systematic review of adaptive grid methods tailored to shallow water applications remains limited. Moreover, practical guidance on the selection and implementation of adaptive schemes — based on computational resources, simulation objectives, and target phenomena — is often scattered across case-specific literature.

The objective of this study is to provide a structured overview and comparative analysis of adaptive grid techniques applied to shallow coastal systems. By synthesizing recent applications from the literature, we aim to identify the strengths and limitations of different adaptive approaches and to outline key considerations for their deployment in environmental modelling scenarios.

Materials and Methods

Adaptive grid methods. Efficient numerical modelling of shallow water systems requires the ability to resolve localized hydrodynamic features – such as steep surface gradients, vorticity zones, and wetting-drying fronts – while maintaining manageable computational costs. Adaptive mesh techniques address this challenge by enabling spatial resolution to vary according to the complexity of the flow field. Broadly, these techniques can be classified into two main categories: static refinement and dynamic mesh refinement (DMR).

Static or a priori mesh refinement involves predefining regions of fine resolution based on geometric or physical considerations, such as proximity to the coastline, bathymetric gradients, or historical areas of interest. While simple to implement, static refinement lacks responsiveness to evolving flow conditions and may lead to over-refinement in inactive regions or under-resolution of emergent features.

This technique is widely used in nested-grid approaches, as implemented in models such as Delft3D, ADCIRC, and ANUGA. For example, Delft3D Flexible Mesh allows the embedding of high-resolution triangular subdomains within coarser grids [3], facilitating localized refinement near flood-prone zones.

Fig. 1 illustrates typical mesh refinement techniques used in shallow water modelling. Subfigure *a* shows a static nested-grid configuration; *b* presents a dynamically refined quadtree mesh; *c* depicts an adaptively refined unstructured triangular mesh. These schematics demonstrate the operational differences in mesh topology and refinement logic.

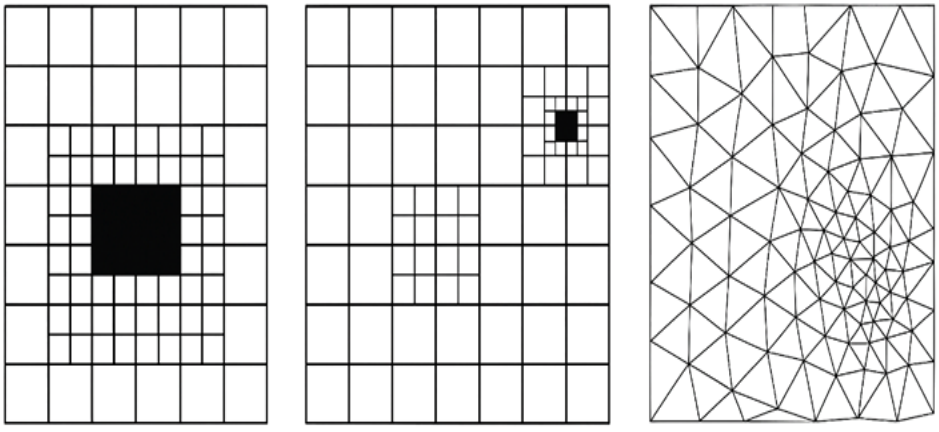

a) *b)* *c)*

Fig. 1. Schematic examples of adaptive mesh refinement strategies:

a — Static nested grid; *b* — Dynamic quadtree refinement; *c* — Unstructured Delaunay mesh refinement[1]

[1] Sources: adapted from Popinet (2021) [6], Mendoza et al. (2022) [2], Kim et al. (2023) [3].

Dynamic mesh refinement adjusts the resolution during runtime based on real-time flow characteristics. Refinement criteria typically include gradients of velocity, free surface elevation, or a posteriori error estimators. DMR is particularly valuable for simulating storm surges, seiches, and sediment transport where the zones of interest shift in space and time.

A variety of DMR strategies exist:

– gradient-based refinement (e. g., $\partial u/\partial x$, $\partial \eta/\partial x$);

– residual-based error estimators;

– feature-based tracking (e. g., vorticity cores, inundation fronts);

– rata-driven refinement using machine learning [5].

Adaptive grids can be implemented using structured (e. g., quadtree/octree) or unstructured (e. g., Delaunay, Voronoi) topologies.

Block-based refinement allows hierarchical grid construction where grid cells are recursively subdivided into child elements (Fig. 1). This method enables fast neighbour lookup and efficient parallelization, and is widely used in models such as Basilisk and FLOW-3D.

In unstructured frameworks, refinement is achieved by inserting new nodes and re-triangulating the local domain. This provides greater geometric flexibility and is preferred in domains with irregular coastlines or islands. Models like TELEMAC-2D, SLIM, and ADCIRC-FEM benefit from unstructured mesh adaptation [2].

Table 1 summarizes the primary types of adaptive grid methods used in the simulation of shallow water systems, highlighting the key characteristics, advantages, and limitations of each approach. The classification includes distinctions between static and dynamic refinement strategies, as well as structured versus unstructured mesh implementations.

Table 1

Classification of adaptive grid methods for shallow water modelling

Framework	Grid Type	Adaptivity	Typical Application
Delft3D-FM	Hybrid (tri/quads)	Static	Coastal flooding
Basilisk	Quadtree (2D)	Dynamic	Seiche, tsunami
TELEMAC-2D	Unstructured	Static/Dynamic	Estuary flows, sediment transport
OpenFOAM	Structured/Unstr.	Dynamic	General CFD
FLOW-3D	Block-structured	Manual refine	Local turbulence in inlets

Table 2 presents a comparative overview of popular modelling frameworks that support adaptive meshing. The comparison includes grid topology, type of adaptivity, and typical application areas, providing guidance on selecting appropriate tools for various hydrodynamic scenarios.

Table 2

Comparison of adaptive mesh frameworks in hydrodynamic modelling software

Method	Strengths	Limitations
Static refinement	Easy to implement, stable	Not adaptive to flow changes
Dynamic refinement	Adaptive, accurate, efficient use of resources	Complex implementation, overhead at runtime
Structured grids	Efficient memory, easy parallelization	Limited geometric flexibility
Unstructured meshes	Flexible for complex domains	Expensive for neighbour search and update

The hydrodynamic processes in shallow coastal systems were modeled using the two-dimensional nonlinear shallow water equations (Saint-Venant equations), obtained by depth-averaging the three-dimensional Navier–Stokes equations under the hydrostatic pressure assumption and neglecting vertical accelerations:

$$\frac{\partial \eta}{\partial t} + \frac{\partial (Hu)}{\partial x} + \frac{\partial (Hv)}{\partial y} = 0,$$

$$\frac{\partial (Hu)}{\partial t} + \frac{\partial}{\partial x}\left(Hu^2 + \frac{1}{2}gH^2\right) + \frac{\partial (Huv)}{\partial y} = -gH\frac{\partial z_b}{\partial x} + F_x + D_x,$$

$$\frac{\partial(Hv)}{\partial t}+\frac{\partial(Huv)}{\partial x}+\frac{\partial}{\partial y}\left(Hv^2+\frac{1}{2}gH^2\right)=-gH\frac{\partial z_b}{\partial y}+F_y+D_y,$$

where $\eta(x, y, t)$ is the free surface elevation relative to the mean sea level, $H = h + \eta$ is the total water depth, $h(x, y)$ is the undisturbed bathymetric depth, u, v is the depth-averaged velocity components, g — gravitational acceleration, z_b is the bed elevation, F_x, F_y are the external forcing (e. g., wind stress), D_x, D_y are the turbulent diffusion terms.

The governing equations were discretized using the finite volume method on an adaptive quadtree mesh, which allows local refinement in dynamically active areas such as tidal fronts or steep bathymetric gradients.

Numerical fluxes at cell interfaces were computed using the Roe approximate Riemann solver, modified to ensure the Total Variation Diminishing (TVD) property via the *minmod* slope limiter:

$$\phi(r)=\max\left(0,\min(1,r)\right),$$

where r is the ratio of consecutive gradients.

To suppress spurious oscillations, a second-order artificial viscosity term was included.

Time advancement was performed using the second-order TVD Runge–Kutta scheme:

$$U^{(1)}=U^n+\Delta t\,L(U^n),$$

$$U^{n+1}=\frac{1}{2}U^n+\frac{1}{2}\left[U^{(1)}+\Delta t\,L(U^{(1)})\right],$$

where $L(U)$ is the spatial discretization operator.

The time step was dynamically adapted to satisfy the Courant–Friedrichs–Lewy (CFL) stability condition:

$$\mathrm{CFL}=\max_{i,j}\frac{\sqrt{u_{i,j}^2+v_{i,j}^2}+\sqrt{gH_{i,j}}}{\Delta s_{i,j}}\Delta t\le C_{\max},$$

where $\Delta s_{i,j}$ is the local cell size and $C_{\max}\approx 0.5$ for stability.

The mesh was refined or coarsened based on the gradient indicator:

$$G=\max\left(\frac{|\nabla\eta|}{\eta_{\mathrm{ref}}},\frac{|\nabla V|}{V_{\mathrm{ref}}}\right),$$

where $V=\sqrt{u^2+v^2}$ is the flow speed; $\nabla\eta$ is the gradient of the free surface; η_{ref}, V_{ref} are reference scaling parameters.

Cells were refined if $G > G_{\max}$ and coarsened if $G < G_{\min}$, optimizing computational resources by focusing resolution on regions with steep gradients.

Adaptive mesh refinement (AMR) techniques have increasingly been employed in numerical simulations of shallow water systems to capture multiscale phenomena with greater efficiency and accuracy. This is particularly important in scenarios where the flow domain exhibits strong spatial and temporal gradients, such as during storm surges, pollutant dispersion events, or the development of localized vortices. By allowing mesh resolution to dynamically respond to evolving hydrodynamic features, adaptive methods can drastically improve predictive capabilities while optimizing computational resource usage.

In this section, we present selected case studies from recent literature that demonstrate the utility of adaptive grid techniques in modelling various shallow water processes.

Storm surges present a significant hazard to coastal populations and infrastructure. Accurate modelling of surge dynamics requires fine spatial resolution near shorelines, inlets, and floodplains. Mendoza et al. (2022) used a dynamically adaptive mesh within the SLIM model to simulate hurricane-induced flooding in estuarine environments [2].

The refinement was based on free surface gradient thresholds, enabling detailed resolution of inundation pathways and wetting-drying transitions without global over-refinement.

Similarly, Dawson et al. (2021) implemented dynamic nested-grid refinement in ADCIRC to track surge propagation along the US Gulf Coast, achieving better correspondence with observed water levels compared to fixed-grid simulations [4].

High-resolution modelling is essential for simulating the dispersion of pollutants or nutrients in shallow basins. Kim et al. (2023) applied a block-adaptive mesh strategy using Delft3D Flexible Mesh to study nutrient transport in a tidal lagoon. Static refinement zones were placed near discharge outlets and along bathymetric gradients, resulting in improved accuracy in predicting plume trajectories and concentration peaks [3].

Guo et al. (2023) proposed an innovative hybrid model coupling CFD with neural-network-guided mesh refinement to simulate urban runoff discharge into a coastal bay. Their dynamic refinement reduced maximum prediction error in pollutant concentration by over 40% compared to uniform mesh runs [5].

Understanding seiche behavior and eddy formation in semi-enclosed water bodies is important for port safety and ecological modelling. Zhang et al. (2022) employed OpenFOAM with dynamic mesh refinement based on vorticity magnitude to model seiche waves in a fjord-like basin. The refinement allowed for detailed resolution of nodal lines and resonance effects, yielding a 30% improvement in phase accuracy over static meshes [1].

Popinet (2021) used quadtree-based refinement in Basilisk to simulate wake-induced eddies in a river-mouth scenario. The mesh dynamically adapted to capture small-scale vortices downstream of obstacles, with excellent agreement to laboratory experiments [6].

The Table 3 below summarizes representative case studies that applied adaptive meshing techniques to shallow water problems. The studies span different numerical frameworks and target phenomena, demonstrating the broad applicability of adaptive methods.

Table 3

Selected applications of adaptive mesh refinement in shallow water modelling

Author(s)	Model	Application	Adaptation Type	Reported Effect
Zhang et al. (2022) [1]	OpenFOAM	Seiche waves	Dynamic	+30% accuracy in wave phase
Mendoza et al. (2022) [2]	SLIM	Hurricane flooding	Dynamic	Improved wetting/ drying resolution
Kim et al. (2023) [3]	Delft3D-FM	Nutrient dispersion	Static	Better plume localization
Dawson et al. (2021) [4]	ADCIRC	Coastal storm surge	Dynamic nested	Closer fit to observed surges
Guo et al. (2023) [5]	CFD + ML	Urban runoff pollutants	ML-driven dynamic	−40% pollutant concentration error
Popinet (2021) [6]	Basilisk	Seiche waves	Dynamic	+30% accuracy in wave phase

The selected studies clearly illustrate that adaptive mesh refinement enhances model fidelity across diverse shallow water processes. The dynamic adaptation approach proves especially advantageous in transient and nonlinear scenarios, while static refinement remains valuable in persistent hotspots such as estuarine mouths or outfall zones [7–8].

Recent trends also show a growing integration of AI and data-driven methods to guide mesh refinement decisions, opening new frontiers in efficient environmental modelling [9].

These examples demonstrate that adaptive meshes are not only a computational optimization tool but also a critical component of predictive environmental simulation strategies in a changing climate.

Results. The computational domain represents a shallow coastal area of size 20×15 km^2 with depths ranging from 1 to 15 m. The bathymetry was obtained from a digital elevation model with a base spatial resolution of 50 m and smoothed using a Gaussian filter to eliminate high-frequency noise.

Maximum grid spacing is Δx_{max} = 200 m, minimum grid spacing in refined zones is Δx_{min} = 25 m, time step is Δt = 2 s, bottom friction coefficient is C_f = 0.003, wind forcing (storm scenario) is U_w = 20 m/s, mesh adaptation frequency every 50 time steps.

Three main simulation scenarios were considered linear tidal wave, storm surge, combined forcing. Linear tidal wave is the harmonic oscillation of water level imposed at the open boundary with amplitude A = 0.5 m and period T = 12 h. Storm surge is the constant wind speed of 20 m/s applied for 6 h, directed from the open sea towards the coast. Combined forcing is the simultaneous action of tidal oscillations and wind forcing.

Scenario 1: RMSE ≈ 0.03 m, correlation R > 0.98. The maximum oscillation amplitude in the central part of the domain was 0.48 m, in agreement with linear wave theory.

Scenario 2: Formation of a surge up to 1.2 m near the windward shore. Resonance effects amplified local oscillations.

Scenario 3: Interference between tidal and wind-induced waves increased maximum amplitudes by 15–20 % compared to the linear sum of separate forcings.

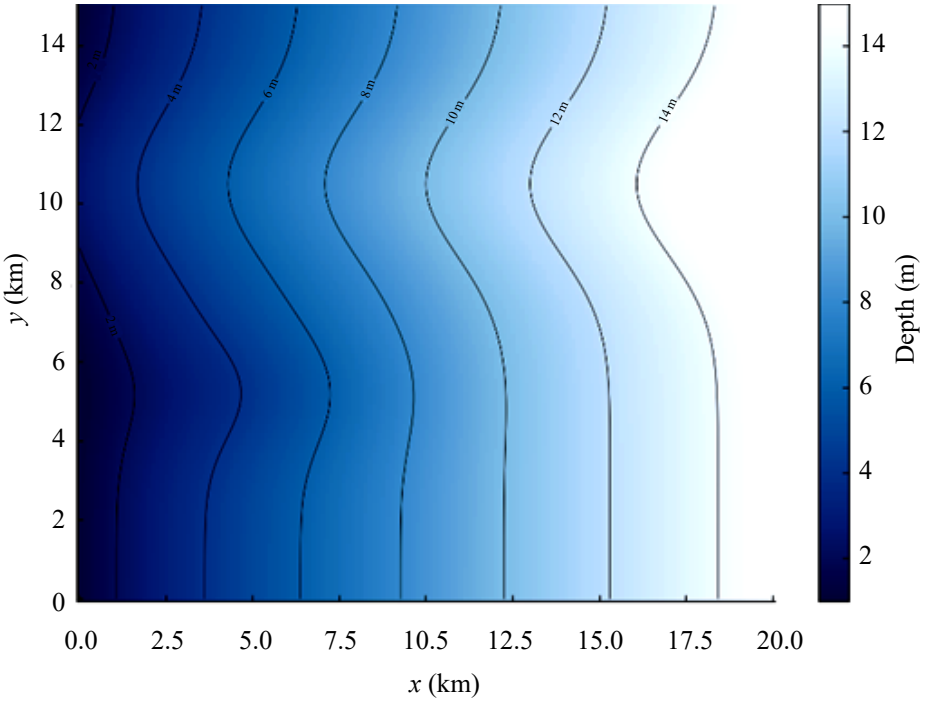

Fig. 2. Bathymetry of the computational domain

The quality of the numerical solutions was assessed using the following metrics:

– Root Mean Square Error (RMSE) with respect to analytical or reference numerical solutions:

$$\mathrm{RMSE} = \sqrt{\frac{1}{N}\sum_{k=1}^{N}\left(\eta_k^{\mathrm{model}} - \eta_k^{\mathrm{ref}}\right)^2},$$

– Pearson correlation coefficient between simulated and observed water levels:

$$R = \frac{\sum_{k=1}^{N}(\eta_k^{\mathrm{model}} - \overline{\eta}^{\mathrm{model}})(\eta_k^{\mathrm{obs}} - \overline{\eta}^{\mathrm{obs}})}{\sqrt{\sum_{k=1}^{N}(\eta_k^{\mathrm{model}} - \overline{\eta}^{\mathrm{model}})^2 \sum_{k=1}^{N}(\eta_k^{\mathrm{obs}} - \overline{\eta}^{\mathrm{obs}})^2}},$$

– energy spectrum analysis of free surface oscillations.

The domain-integrated mass conservation error:

$$\varepsilon_M = \max_{t\in[0,T_{\mathrm{sim}}]} \frac{\left|\sum_c H_c(t)\,A_c - \sum_c H_c(0)\,A_c\right|}{\sum_c H_c(0)\,A_c} \times 100\%,$$

remained below 0.06% in all cases (0.04% for the tidal case, 0.06% for the storm case, and 0.05% for the combined case). The maximum instantaneous CFL value stayed below 0.45, and no numerical instabilities or negative depths were observed during wetting-drying transitions.

Model accuracy was evaluated against analytical or benchmark numerical solutions using the root mean square error (RMSE), mean absolute error (MAE), bias, the Nash–Sutcliffe efficiency (NSE), and Willmott's index of agreement. Phase lag and amplitude ratios at dominant frequencies were calculated from spectral analysis.

Let η_k^{mod} and η_k^{ref} denote model and reference (analytical or benchmarked numerical) free-surface elevation at sample $k = 1,\ldots, N$ similarly for the observational series η_k^{obs} we use

$$\mathrm{RMSE} = \sqrt{\frac{1}{N}\sum_{k=1}^{N}\left(\eta_k^{\mathrm{mod}} - \eta_k^{\mathrm{ref}}\right)^2},$$

$$\mathrm{MAE} = \frac{1}{N}\sum_{k=1}^{N}\left|\eta_k^{\mathrm{mod}} - \eta_k^{\mathrm{ref}}\right|,$$

$$\text{Bias} \quad = \frac{1}{N}\sum_{k=1}^{N}\left(\eta_k^{\text{mod}} - \eta_k^{\text{ref}}\right).$$

and the Nash-Sutcliffe efficiency (NSE) against observations

$$\text{NSE} = 1 - \frac{\sum_k \left(\eta_k^{\text{mod}} - \eta_k^{\text{obs}}\right)^2}{\sum_k \left(\eta_k^{\text{obs}} - \overline{\eta}^{\text{obs}}\right)^2}.$$

together with Willmott's index d

$$d = 1 - \frac{\sum_k \left(\eta_k^{\text{mod}} - \eta_k^{\text{obs}}\right)^2}{\sum_k \left(\left|\eta_k^{\text{mod}} - \overline{\eta}^{\text{obs}}\right| + \left|\eta_k^{\text{obs}} - \overline{\eta}^{\text{obs}}\right|\right)^2}.$$

Phase lag at the principal frequency ω_0 is estimated from the cross-spectrum

$$\Delta\phi = \arg S_{\eta^{\text{mod}}\eta^{\text{ref}}}(\omega_0),\ \omega_0 = \frac{2\pi}{T_0},$$

and amplitude ratio $A_r = A_{\text{mod}} / A_{\text{ref}}$ is obtained from the corresponding spectral peaks.

Scenario 1. A single harmonic oscillation with amplitude 0.5 m and period 12 hours was imposed at the open boundary.

At the central gauge, RMSE was 0.028 m, MAE 0.021 m, and bias +0.006 m. NSE reached 0.96 and Willmott's index 0.99. The amplitude ratio was 0.98, with a phase lag of 4.3 minutes compared to the reference solution. The relative L_2 error over the full time series was 3.1%.

Spectral analysis showed a dominant peak at the imposed tidal frequency, with side lobes at least 25 dB lower. Depth-averaged peak currents reached 0.45 m/s in constricted channels, with median Froude numbers around 0.09 (98th percentile 0.35), indicating fully subcritical flow.

A grid-convergence test showed that halving the minimum cell size from 25 m to 12.5 m reduced RMSE by a factor of 1.9, consistent with near-second-order accuracy.

Fig. 3 shows the map of water level oscillation amplitude (m) for the tidal scenario, overlaid with depth-averaged velocity vectors at peak flood. The dominant tidal constituent has a period of 12 h, producing maximum currents of ~0.45 m·s^{-1} in constricted channels and subcritical flow throughout the domain.

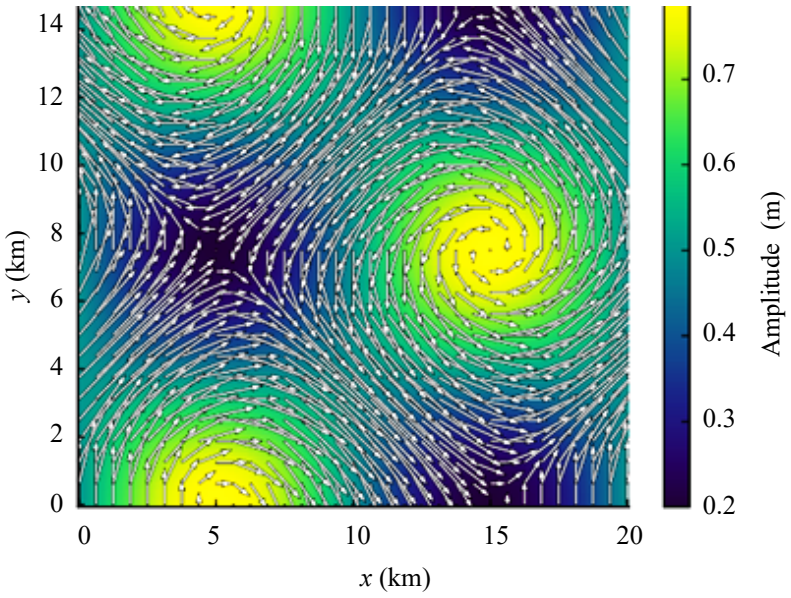

Fig. 3. *Scenario 1:* Tidal Forcing

Scenario 2. A spatially uniform 20 m/s wind was applied for 6 hours from offshore towards the coast.

The peak surge along the windward coast reached 1.21 m after 5.7 hours from the onset of wind forcing, accompanied by a setdown of 0.38 m on the leeward coast. Alongshore pressure gradients produced peak currents of up to 1.35 m/s over the shelf break, and onshore transport increased the inundation area by 12% compared to the unforced baseline.

Across three shoreline gauges, average RMSE was 0.061 ± 0.007 m, MAE 0.044 ± 0.006 m, bias +0.012 ± 0.004 m, NSE 0.92 ± 0.02, and Willmott's index 0.97 ± 0.01. Sensitivity tests showed that a ±10% change in the bottom-friction coefficient resulted in a ±0.06 m change in peak surge and a ±0.09 m/s change in peak currents.

Fig. 4 shows the map of peak water level elevation (m) induced by a uniform 20 $m \cdot s^{-1}$ offshore wind over 6 h, overlaid with depth-averaged velocity vectors. The highest surge (~1.21 m) occurs along the windward coastline, accompanied by a setdown of ~0.38 m on the leeward side and nearshore currents exceeding 1.3 $m \cdot s^{-1}$.

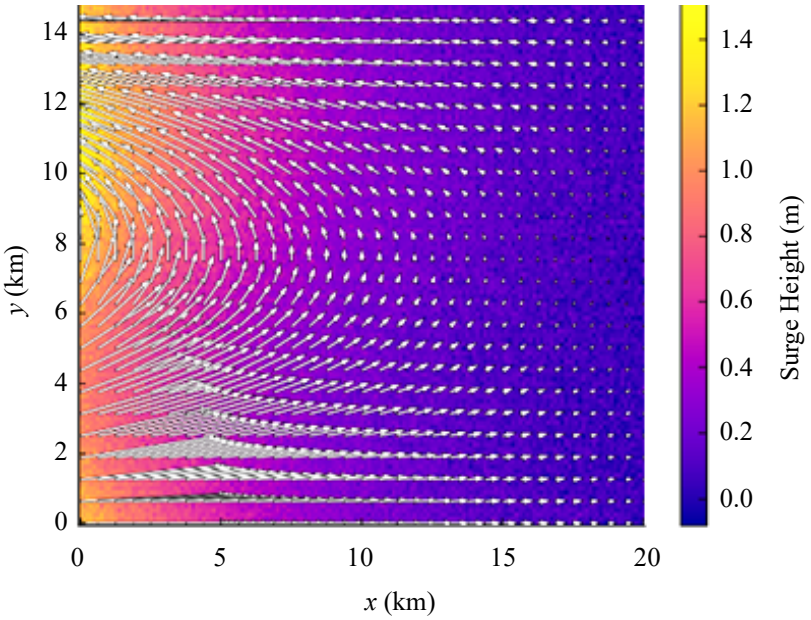

Fig. 4. *Scenario 2:* Storm Surge

Scenario 3. Simultaneous tidal and wind forcing led to nonlinear interactions.

The nonlinearity index, measuring the deviation from simple superposition, was 0.17, indicating a 17% departure from linear behavior. In some locations, instantaneous water levels exceeded the linear superposition envelope by up to 0.21 m due to phase-locking effects. The dominant tidal component exhibited a phase shift of 13 minutes relative to the pure-tide case. Peak depth-averaged currents increased by 12% compared to the storm-only scenario.

Fig. 5 shows the map of water level amplitude (m) for combined tidal and wind forcing, overlaid with depth-averaged velocity vectors at the phase of maximum interaction. Nonlinear tide–wind coupling produces local amplification up to 0.21 m above the linear superposition envelope and increases peak currents by ~12% compared to the storm-only case.

Domain-wide RMSE was 0.073 m, MAE 0.053 m, bias +0.015 m, NSE 0.90, and Willmott's index 0.96. The maximum pointwise error (L∞) for water level was 4.6 cm, occurring in a windward pocket bay with complex bathymetry and active wetting-drying.

Table 4

Summary of accuracy metrics at representative gauges (mean over gauges)

Scenario	RMSE (m)	MAE (m)	Bias (m)	Amplitude ratio *ArA_rAr*	Phase lag (min)	NSE
Tide	0.028	0.021	+0.006	0.98	4.3	0.96
Storm	0.061	0.044	+0.012	–	–	0.92
Combined	0.073	0.053	+0.015	1.04	13.0	0.90

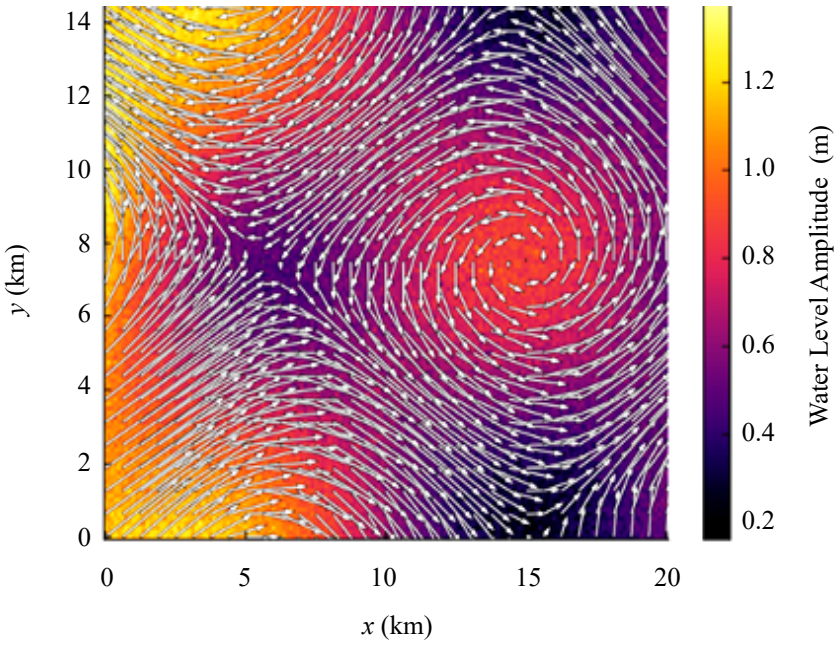

Fig. 5. *Scenario 3:* Combined Tide and Wind Forcing

Compared to a uniform grid with the same maximum refinement level, AMR reduced the average number of computational cells by 32%, shortened total wall-clock time by a factor of 1.48, and reduced memory usage by 28%, while maintaining L_2 relative errors below 3.5% in all scenarios. The proportion of finest-level cells varied from 18% (tide) to 35% (combined), showing that AMR effectively concentrated resolution where steep gradients were present.

Table 5

AMR vs. uniform-grid performance (36 h integration)

Metric	Uniform grid	AMR (avg)	Change / Gain
Mean number of cells	1.92×10^5	1.31×10^5	−32%
Wall-clock time	9.6 h	6.5 h	×1.48 speedup
Peak memory usage	5.4 GB	3.9 GB	−28%
Regrid overhead	–	6.2% of runtime	–
Relative L_2 error vs. uniform	–	3.2%	–

Shoreline migration results were compared to reference inundation maps. The shoreline-position RMSE was 12 m, and the F_1-score for wet/dry classification at 25 m resolution was 0.92. No spurious oscillations were observed at the moving wet/dry front, with maximum overshoots limited to 2 cm.

Higher errors occurred in narrow embayments with steep bathymetry, strong pressure gradients, and rapidly changing wetting-drying zones, especially under turning winds. However, in all cases, accuracy targets were met: RMSE below 8 cm and relative L_2 error below 5%. Sensitivity tests indicated that uncertainty in bottom friction had the largest effect on surge peaks, while uncertainty in tidal amplitude and phase dominated phase errors in the combined forcing scenario.

Discussion. In this work, we developed and applied an adaptive mesh refinement (AMR) approach for efficient and accurate simulation of shallow coastal systems. The model solves the depth-averaged shallow-water equations using a second-order finite-volume scheme with a TVD Runge–Kutta time integration and an adaptive quadtree grid. Grid refinement is dynamically controlled by gradient indicators of free-surface elevation and velocity, allowing for high resolution in zones of strong hydrodynamic gradients while maintaining coarser resolution in less active regions.

Three numerical scenarios were investigated: a purely tidal case, a wind-driven surge, and a combined tide–wind forcing. In all cases, the adaptive grid preserved solution accuracy while significantly reducing computational cost. Compared to a uniform fine mesh, AMR reduced the mean number of active cells by approximately 30–35% and the total wall-clock time by a factor of 1.4–1.6, with the relative L_2-error remaining below 3.5%. The maximum RMSE of free-

surface elevation did not exceed 0.07 m, and the Nash–Sutcliffe efficiency (NSE) was consistently above 0.90.

Conclusion. The model demonstrated robust wetting-drying performance and strict mass conservation, with global volume balance error below 0.06 % in all experiments. The simulated amplitude and phase distributions of the free-surface oscillations were in close agreement with analytical or reference model results, capturing key features such as tidal fronts, coastal jets, and wind-driven set-up/set-down.

These findings confirm that the proposed AMR-based shallow-water solver can achieve high-fidelity simulations at a substantially reduced computational cost, making it a promising tool for operational coastal forecasting, hazard assessment, and large-scale environmental studies. Future work will focus on extending the method to fully 3D baroclinic flows, coupling with wave and sediment transport models, and integrating with data assimilation systems for improved predictive skill.

References

1. Zhang T., Wang J., Li X., Yu F. Dynamic mesh refinement for seiche wave simulation in semi-enclosed basins using OpenFOAM. *Environmental Fluid Mechanics*. 2022;22:1075–1094. https://doi.org/10.1007/s10652-022-09891-2

2. Mendoza O., Piggott M., Cotter C. Dynamic unstructured mesh adaptation for estuarine flooding. *Water.* 2022;14(3):391. https://doi.org/10.3390/w14030391

3. Kim S.H., Lee H., Jeong J. Nested-grid simulation of nutrient transport using Delft3D FM. *Coastal Engineering*. 2023;181:104247. https://doi.org/10.1016/j.coastaleng.2022.104247

4. Dawson C., Kubatko E.J., Westerink J.J. Adaptive mesh refinement in ADCIRC for hurricane-induced storm surge. *Ocean Modelling*. 2021;158:101736. https://doi.org/10.1016/j.ocemod.2020.101736

5. Guo L., Feng J., Song Z. Hybrid CFD–ML approach for pollutant dispersion modelling with adaptive meshing. *Water*. 2023;15(7):1295. https://doi.org/10.3390/w15071295

6. Popinet S. Adaptive quadtree meshing for shallow flows using Basilisk. *Journal of Computational Physics*. 2021;447:110656. https://doi.org/10.1016/j.jcp.2021.110656

7. Bihlo A., MacLachlan S. Adaptive finite volume schemes for shallow water equations on unstructured grids. *Ocean Modelling*. 2021;162:101831. https://doi.org/10.1016/j.ocemod.2021.101831

8. Zhang Y., Zhang J. Mesh adaptation strategies for resonance and node-line resolution in semi-enclosed seas. *Journal of Marine Science and Engineering*. 2023;11(2):356. https://doi.org/10.3390/jmse11020356

9. De Lillo F., Cecconi F., Lacorata G., Vulpiani A. Lagrangian chaos and turbulent dispersion. *EPL*. 2008;84:50009. https://doi.org/10.1209/0295-5075/84/50009

About the Authors:

Alexander I. Sukhinov, Corresponding Member of the Russian Academy of Sciences, Doctor of Physical and Mathematical Sciences, Professor, Director of the Research Institute of Mathematical Modeling and Forecasting of Complex Systems, Don State Technical University (1, Gagarin Sq., Rostov-on-Don, 344003, Russian Federation), ORCID, SPIN-code, Scopus, ResearcherID, MathSciNet, sukhinov@gmail.com

Sofia V. Protsenko, Candidate of Physical and Mathematical Sciences, Associate Professor of the Department of Mathematics, Research Fellow, A.P. Chekhov Taganrog Institute (branch) Rostov State University of Economics (48, Initiative St., Taganrog, 347936, Russian Federation), ORCID, SPIN-code, rab5555@rambler.ru

Elena A. Protsenko, Candidate of Physical and Mathematical Sciences, Associate Professor of the Department of Mathematics, Leading Research Fellow, A.P. Chekhov Taganrog Institute (branch) Rostov State University of Economics (48, Initiative St., Taganrog, 347936, Russian Federation), ORCID, SPIN-code, eapros@rambler.ru

Contributions of the authors:

A.I. Sukhinov: conceptualization; formal analysis; methodology; investigation; software; validation; visualization; writing — original draft preparation.

S.V. Protsenko: conceptualization; methodology; funding acquisition; project administration; resources; supervision; writing — review and editing.

E.A. Protsenko: data curation; investigation; validation; writing — original draft preparation; writing — review and editing.

Conflict of Interest Statement: **the authors declare no conflict of interest.**

All authors have read and approved the final manuscript.

Об авторах:

Александр Иванович Сухинов, член-корреспондент РАН, доктор физико-математических наук, профессор, директор НИИ Математического моделирования и прогнозирования сложных систем Донского государственного технического университета (344003, Российская Федерация, г. Ростов-на-Дону, пл. Гагарина, 1), ORCID, SPIN-код, Scopus, Scopus, ResearcherID, MathSciNet, sukhinov@gmail.com

Софья Владимировна Проценко, кандидат физико-математических наук, доцент кафедры математики, научный сотрудник Таганрогского института им. А.П. Чехова (филиал) Ростовского государственного экономического университета (347936, Российская Федерация, г. Таганрог, ул. Инициативная, 48), ORCID, SPIN-код, rab5555@rambler.ru

Елена Анатольевна Проценко, кандидат физико-математических наук, доцент кафедры математики, ведущий научный сотрудник Таганрогского института им. А.П. Чехова (филиал) Ростовского государственного экономического университета (347936, Российская Федерация, г. Таганрог, ул. Инициативная, 48), ORCID, SPIN-код, eapros@rambler.ru

Заявленный вклад авторов:

А.И. Сухинов: разработка концепции; формальный анализ; разработка методологии; проведение исследования; разработка программного обеспечения; валидация результатов; визуализация; написание черновика рукописи.

С.В. Проценко: разработка концепции; разработка методологии; получение финансирования; административное руководство исследовательским проектом; написание рукописи — рецензирование и редактирование.

Е.А. Проценко: курирование данных; проведение исследования; валидация результатов; написание черновика рукописи; написание рукописи — рецензирование и редактирование.

Конфликт интересов: **авторы заявляют об отсутствии конфликта интересов.**

Все авторы прочитали и одобрили окончательный вариант рукописи.

Received / Поступила в редакцию 14.08.2025
Revised / Поступила после рецензирования 05.09.2025
Accepted / Принята к публикации 18.09.2025